Physica B 176 (1992) 33–53
North-Holland

PHYSICA B

Field applied molecular dynamics (FMD) simulation of the inverse Faraday effect

M.W. Evans[1], S. Woźniak[2] and G. Wagnière

Institute of Physical Chemistry, University of Zurich, Winterthurerstrasse 190, CH-8057 Zurich, Switzerland

Received 19 April 1991
Revised manuscript received 19 June 1991

The inverse Faraday effect, magnetisation due to a circularly polarised pump laser, is simulated by field applied molecular dynamics (FMD). The FMD method produces two main results: (a) dynamic magnetisation (a finite $t \to \infty$ value of the angular momentum time autocorrelation function, and (b) finite second order rise transients due to the rotating torque of a laser pulse applied in the simulation on the femtosecond time scale. These and other features of the laser-on molecular dynamics are intricate functions of the pump laser frequency in the experimentally accessible visible range. Results are given for a diamagnetic chiral D_2 molecular symmetry (bicyclopropene), and a diamagnetic achiral C_{2v} molecular symmetry, water.

1. Introduction

The ability of an intense, circularly polarised, pump laser to produce bulk magnetisation was first predicted theoretically by Pershan [1] and demonstrated in a series of novel experiments by Van der Ziel et al. [2, 3], both in low temperature paramagnetic glasses and in room temperature diamagnetic liquids with high Verdet constants [4]. The magnetisation was named [1–3] the inverse Faraday effect (IFE). The IFE was later developed theoretically by Atkins and Miller [5] and is summarised in textbooks by Atkins [6] and Shen [7], the latter in terms similar to the optical Stark effect [8–10]. It was later shown by Wagnière [11] and by Woźniak and co-workers [12–15] that the theory of the IFE can be developed in terms of the antisymmetric part of the tensor product $\boldsymbol{E}_i \boldsymbol{E}_j^*$ of electric field components of the laser. Here the symbol $\boldsymbol{E}_j^*$ denotes the complex conjugate of $\boldsymbol{E}_j$, using subscript (tensor) notation. The conjugate product is conveniently defined as

$$\boldsymbol{\Pi}_{ij}^{\mathrm{A}} = \tfrac{1}{2}(\boldsymbol{E}_i \boldsymbol{E}_j^* - \boldsymbol{E}_j \boldsymbol{E}_i^*) ,$$
$$\boldsymbol{\Pi}_i^{\mathrm{A}} = \varepsilon_{ijk} \boldsymbol{\Pi}_{jk}^{\mathrm{A}} , \qquad (1)$$

where $\boldsymbol{\varepsilon}_{ijk}$ is the third rank antisymmetric unit tensor. In this notation, $\boldsymbol{\Pi}_{ij}^{\mathrm{A}}$ is a polar, second rank, antisymmetric tensor, and $\boldsymbol{\Pi}_i^{\mathrm{A}}$ is a rank one axial tensor, i.e. an axial vector. Both the tensor $\boldsymbol{\Pi}_{ij}^{\mathrm{A}}$ and the vector $\boldsymbol{\Pi}_i^{\mathrm{A}}$ represent the same physical quantity. The tensor $\boldsymbol{\Pi}_{ij}^{\mathrm{A}}$ or vector $\boldsymbol{\Pi}_i^{\mathrm{A}}$ are both negative to motion reversal (T) and positive to parity inversion (P). It is particularly fruitful to think of the vector representation $\boldsymbol{\Pi}_i^{\mathrm{A}}$ in the same terms as static magnetic flux density B_i^0, which has precisely the same [16–20] symmetry characteristics. Using this basic symmetry analogy has led to the prediction of an inverse Zeeman effect [16]; a forward–backward birefringence due to $\boldsymbol{\Pi}_i^{\mathrm{A}}$ [17, 18]; and optical NMR and EPR [19, 20], in which a circularly polarised

[1] Permanent address: 433 Theory Center, Cornell University, Ithaca, NY 14853, USA.
[2] Permanent address: Nonlinear Optics Division, Institute of Physics, Adam Mickiewicz University, 60-780 Poznań, Poland.

0921-4526/92/$05.00 © 1992 – Elsevier Science Publishers B.V. All rights reserved

laser is directed into the sample tube of a contemporary NMR or EPR spectrometer [19], causing extra magnetisation and analytically useful spectral features due to the combined effect of $\boldsymbol{\Pi}_i^{\mathrm{A}}$ of the laser and B_i^0 of the instrument's permanent magnet. Optical NMR and EPR are potentially of widespread interest [20] and illustrate the useful gedankexperiment [16–20] based on the exact symmetry analogy between $\boldsymbol{\Pi}_i^{\mathrm{A}}$ (a non-linear optical property) and B_i^0.

Pacing these developments chronologically has been the progress in field applied molecular dynamics (FMD) computer simulation. The FMD technique was initiated [21–26] with static electric fields (E_i^0) and generated successfully a range of results, including thermodynamic Langevin and Kielich functions with which to test the FMD method. The same FMD trajectories were used to produce a range of related fundamental results, including: field applied statistical analysis [21, 22] in terms of time correlation functions; field decoupling [23], fall transient acceleration [24], and rise transient oscillation phenomena [25, 26], all indicating specific and fundamental non-linearities of the diffusion process [27]; field induced dynamical effects [28] measured statistically through a set of novel time cross-correlation functions, and other features summarised in ref. [29]. The combined results of numerous FMD runs produced the principles of group theoretical statistical mechanics (GTSM) [30], which led in turn to novel computer analysis of microrheology [31]. GTSM has recently been reviewed in the broader context of fundamental symmetries in physics [32]. FMD has been extended for use with circularly polarised pump lasers [33] and recently to non-linear optical effects [34–36] in general. In doing so, a torque due to the interaction of the external optical field with a molecular property tensor (such as an induced electric or magnetic dipole moment) is coded into the forces loop [37, 38] of any convenient MD algorithm, and the influence of the torque evaluated numerically over the required number of time steps. The integral of the external torque with respect to configuration is the extra term in the Hamiltonian due to the applied field, so that the method is perfectly general, and can be used whenever an external field forms a torque with a molecular property (the arm of the torque).

In this paper, the computer simulation of the IFE proceeds through a torque described in section 2. This is incorporated in FMD as described in section 3. Section 4 illustrates novel second order rise transients due to the IFE, which describe what appears to be a fundamentally new type of non-equilibrium response of the molecular ensemble, illustrated in this work through the IFE torque, but which exists in general. Section 5 is a statistical analysis of the molecular dynamics of two types of molecular ensemble in the post transient steady state (the statistically stationary state in the presence of the pump laser). Results are presented for a paramagnetic chiral ensemble of staggered bicyclopropene molecules and an achiral diamagnetic ensemble of water molecules, showing in each case a novel phenomenon named "dynamic magnetisation". This is measured through the development in response to the pump laser's conjugate product of a finite $t \rightarrow \infty$ level of the angular momentum time autocorrelation function (ACF), a level which is intricately dependent on the applied laser frequency in the visible range accessible to contemporary pump lasers such as the Nd:YAG systems.

2. The torque

The IFE is mediated through the time dependent torque (in vector notation)

$$\boldsymbol{T} = -\boldsymbol{m}^{(\mathrm{ind})} \times \boldsymbol{B}^{(\mathrm{em})} , \tag{2}$$

where $\boldsymbol{B}^{(\mathrm{em})}$ is the magnetic flux density of the electromagnetic plane wave, and $\boldsymbol{m}^{(\mathrm{ind})}$ the induced magnetic dipole moment

$$m_i^{(\mathrm{ind})} = i\, {}^{m}\alpha_{ijk}^{nee} \boldsymbol{\Pi}_{jk}^{\mathrm{A}} . \tag{3}$$

The inverse Faraday effect polarisability tensor ${}^{m}\boldsymbol{\alpha}^{nee}({}^{m}\alpha_{ijk}^{nee} \equiv {}^{m}\alpha_{ijk}^{nee}(0; \omega, -\omega))$ is antisymmetric

with respect to the exchange of the last two indices:

$$ {}^{m}\alpha^{nee}_{ijk}(0;\omega,-\omega) = -{}^{m}\alpha^{nee}_{ikj}(0;\omega,-\omega) \qquad (4) $$

and

$$ {}^{m}\alpha^{nee}_{ijk}(0;\omega,-\omega) = -{}^{m}\alpha^{nee}_{ijk}(0;-\omega,\omega)\,. \qquad (5) $$

As shown elsewhere in detail [39], the frequency dependence of the polarisability ${}^{m}\boldsymbol{\alpha}^{nee}(0;\omega,-\omega)$ leads to a significant enhancement of static magnetisation near optical resonance. On the other hand, if the IFE is investigated far from resonance and damping is neglected, it can be described by the usual Faraday effect polarisability tensor ${}^{e}\boldsymbol{\alpha}^{nem}(-\omega;\omega,0)$ with [12]

$$ {}^{m}\alpha^{nee}_{ijk}(0;\omega,-\omega) = {}^{e}\alpha^{nem}_{kji}(-\omega;\omega,0)\,. \qquad (6) $$

The perturbation calculus of the molecular property tensor ${}^{m}\alpha^{nee}_{ijk}$ has been developed by Wagnière [11], and Woźniak and co-workers [12–15], and its properties close to resonance have been investigated recently by Woźniak et al. [39], showing that the IFE is replete with useful spectral detail. For a left circularly polarised laser propagating in the Z axis, and for D_2 or C_{2v} symmetry molecular point groups [40] the $\boldsymbol{m}^{(ind)}$ components in the frame (1, 2, 3) of the principal molecular moments of inertia reduce to the relatively simple

$$ \begin{aligned} m_1^{(ind)} &= 2e_{1Z}\,{}^{m}\alpha^{nee}_{123}E_0^2\,, \\ m_2^{(ind)} &= 2e_{2Z}\,{}^{m}\alpha^{nee}_{231}E_0^2\,, \\ m_3^{(ind)} &= 2e_{3Z}\,{}^{m}\alpha^{nee}_{312}E_0^2\,, \end{aligned} \qquad (7) $$

in which there are only three independent tensor elements to consider. From (2) and (7) the torque is formed in frame (1, 2, 3) for each molecule of the FMD ensemble and finally back transformed [34] into the laboratory frame (X, Y, Z) using a rotation matrix of unit vectors $\boldsymbol{e}_1$, $\boldsymbol{e}_2$, and $\boldsymbol{e}_3$ in axes 1, 2, and 3, respectively [35, 36]. In this notation the Z component of $\boldsymbol{e}_1$ in the laboratory frame is e_{1Z}, the Y component of $\boldsymbol{e}_1$ is e_{1Y}: the Z component of $\boldsymbol{e}_2$ is e_{2Z} and so on. The quantity $\langle e_{1Z}\rangle$ is therefore the average over 108 molecules of e_{1Z}. Similarly for $\langle e_{1Y}\rangle$ and so on.

The torque takes effect as a function of the product $E_0^2B_0$ of the scalar electric (E_0) and magnetic (B_0) amplitudes of the pump laser field. Coded into the forces loop of the FMD program, it has generated in this work novel rise transients at second and higher even order, exemplified by $\langle e_{1Z}^{2n}\rangle$, $\langle e_{2Z}^{2n}\rangle$, and $\langle e_{3Z}^{2n}\rangle$; which are intricately dependent (section 4) on the applied (visible) pump laser frequency. There are no first or higher odd order equivalents of these second order transients from the same FMD trajectories, and $\langle e_{iZ}^{2n}\rangle$ of the IFE appear to be novel non-equilibrium ensemble properties inaccessible to conventional equilibrium thermodynamic averaging techniques (Langevin function analysis [41]) because the required time averaged IFE energy vanishes. This is explored further in section 4.

The transient state eventually reaches a laser-on steady state, which is statistically stationary [42]. In this condition the FMD samples used in this work have been analysed statistically using a range of appropriate time (ACFs) and cross-correlation functions (CCFs) of molecular dynamical properties such as angular momentum, orientation, rotational velocity [42], and the time derivative of orientation. The analysis was completed at several (up to twenty) laser frequencies in the hundred terahertz range, thus generating a data bank of information, and is summarised in section 5.

3. FMD methods

The FMD method was applied with ensembles of chiral and achiral diamagnetic molecules, staggered bicyclopropene (D_2) and water (C_{2v}), respectively. A level of approximation represented by Lennard–Jones site–site interactions was used for this first simulation of the IFE. It is emphasised that the FMD can be used with other levels of approximation, such as intermolecular parameters modelled ab initio [43], and with any suit-

able type of MD algorithm [44]. The Lennard–Jones level was considered adequate for this demonstration work.

3.1. *Staggered bicyclopropene (e_1 in D_2 axis)*

Bicyclopropene was considered in a chiral, frozen staggered, conformation with one ring permanently at 45° to the other. The intermolecular potential was constructed from six Lennard–Jones CH sites, as in a parallel simulation [40] of the new phenomenon [35] of dynamic polarisation

$$\varepsilon/k(\mathrm{CH}) = 158\ \mathrm{K}\,, \quad \sigma(\mathrm{CH}) = 3.8\ \text{Å}\,. \tag{8}$$

3.2. *Water (e_1 in C_{2v} axis)*

The intermolecular potential in this case was a modified ST2 [45], well tested against the MCYL ab initio flexible potential [46] and against a wide range of experimental data on water [47] in its various forms:

$$\begin{aligned}
&\varepsilon/k(\mathrm{H\text{–}H}) = 21.1\ \mathrm{K}\,, \quad \sigma(\mathrm{H\text{–}H}) = 2.25\ \text{Å}\,,\\
&\varepsilon/k(\mathrm{O\text{–}O}) = 58.4\ \mathrm{K}\,, \quad \sigma(\mathrm{O\text{–}O}) = 2.80\ \text{Å}\,,\\
&q_{\mathrm{H}} = 0.23|e|\,, \quad q(\text{lone pair}) = -0.23|e|\,,\\
&q_{\mathrm{O}} = 0\,,\\
&e = \text{electronic charge}\,.
\end{aligned} \tag{9}$$

Rise transients in both ensembles were computed from an equilibrated sample, applying the torque (2) at $t = 0$ for as many time steps as needed to achieve the laser-on steady state. In the later condition, time correlation functions were computed by running time averaging over a minimum of 6000 time steps each, giving good statistics, since the ACFs and CCFs are typically damped out in about 400 time steps.

These FMD simulations were carried out at 293 K, 1.0 bar, using a time step of 5.0 fs for bicyclopropene, and 0.5 fs for water. Temperature rescaling was used to thermostat the sample, and for some data sets, animation on video was used to analyse the molecular motion by direct visualisation at the Cornell Theory Center, following "sendfile" satellite transmission of data sets. The FMD simulation was repeated at up to twenty different visible laser frequencies for each sample, and for a range of values of the product $E_0^2 B_0$. Animation revealed clearly that an important primary effect of the torque in the IFE in terms of molecular motion is the laser driven precession of molecular dynamical quantities such as angular momentum.

In the absence of ab initio or experimental data on the scalar elements of the mediating tensor ${}^{m}\alpha_{ijk}^{nee}$ of the IFE, the following numbers were coded into the FMD program

$${}^{m}\alpha_{123}^{nee} : {}^{m}\alpha_{231}^{nee} : {}^{m}\alpha_{312}^{nee} = 1:2:3\,. \tag{10}$$

A much more adequate appreciation of these elements is needed, using, for example, a software package such as HONDO [43].

4. Even order rise transients of the IFE

For both samples, second and higher even order rise transients were observed to develop in response to the torque (2), but odd order transients vanished in the "computer noise". Even order rise transients are defined in general by $\langle e_{1Z}^{2n} \rangle$ and so on, where n is a positive definite integer. The FMD method mimicks a laser pulse by switching on a torque at a given time step, a process which by definition takes place over only one time step. The laser pulse therefore rises from zero to its final value in one time step, which for staggered bicyclopropene was 5.0 fs, and for water 0.5 fs. The characteristic rise time of the rise transient following the imposition of this torque was observed to be not shorter than of the order of 100 time steps, and usually of the order 1000 time steps. In comparison the rise time of the laser is therefore approximately a delta function, and the pulse can be regarded as a step function on the time scale of the rise transient. The sequence of results in fig. 1 shows that the even order transients are sensitive functions of applied laser frequency in the visible range, and of the applied laser intensity, proportional to E_0^2. Figure 1 shows that the IFE is accompanied by the development of second order orientational anisotropy through the torque (2). However, integration of this torque with respect to the orientation to give the potential energy

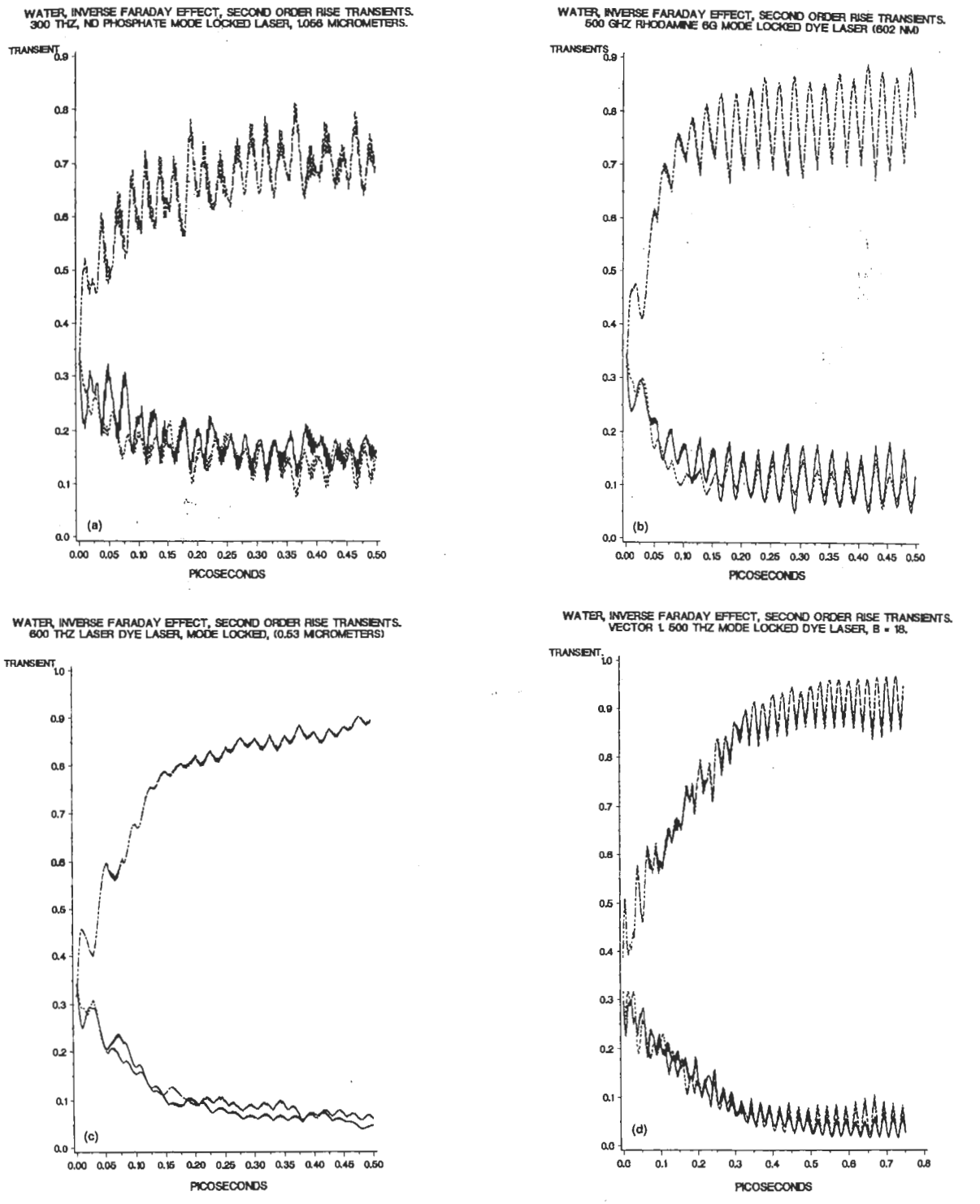

Fig. 1. Second order rise transients ——— $\langle e_{1X}^2 \rangle$, − − − $\langle e_{1Y}^2 \rangle$, and − · · − · · − · · $\langle e_{1Z}^2 \rangle$, IFE. Vector 1 is in the axis of the permanent electric dipole moment of water, and vector 2 is perpendicular and in the plane of the molecule. Vector 3 is mutually perpendicular through the center of mass. (a) 300 THz laser, water; (b) 500 THz laser, water; (c) 600 THz laser, water; (d) as for (c), increased laser intensity; (e) as for (d), vector 2; (f) as for (d), increased laser intensity; (g) 30 THz laser.

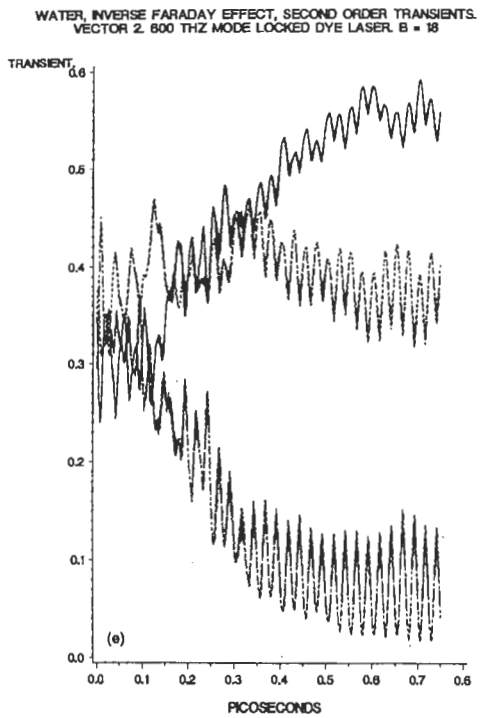
WATER, INVERSE FARADAY EFFECT, SECOND ORDER TRANSIENTS.
VECTOR 2. 600 THZ MODE LOCKED DYE LASER. B = 18
TRANSIENT
(e)
PICOSECONDS

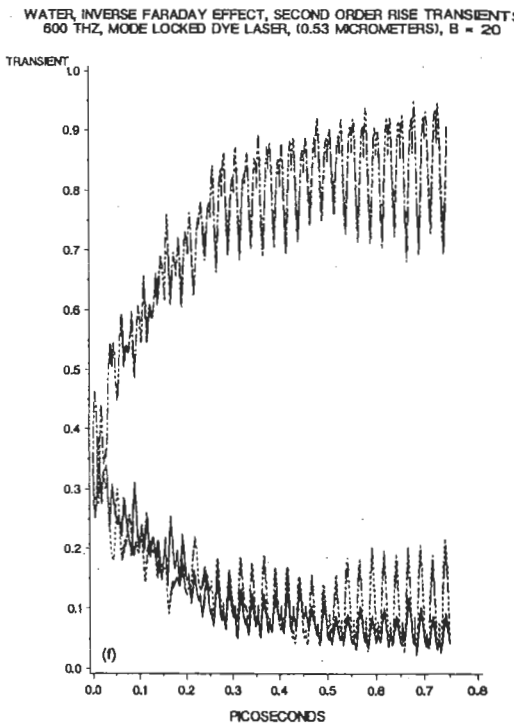
WATER, INVERSE FARADAY EFFECT, SECOND ORDER RISE TRANSIENTS.
600 THZ, MODE LOCKED DYE LASER, (0.53 MICROMETERS), B = 20
TRANSIENT
(f)
PICOSECONDS

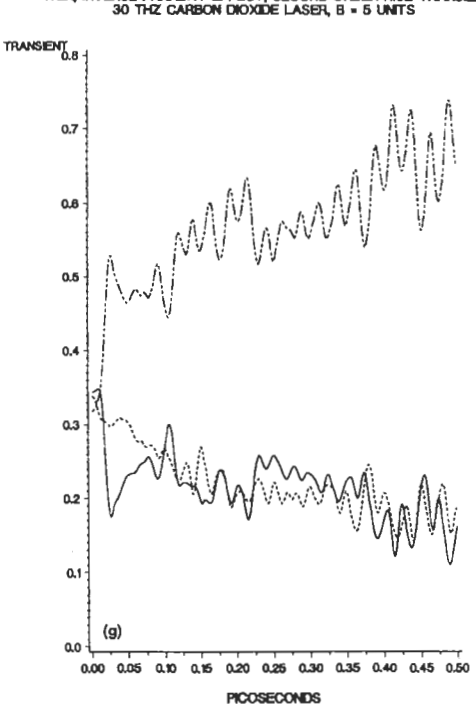
WATER, INVERSE FARADAY EFFECT, SECOND ORDER RISE TRANSIENTS.
30 THZ CARBON DIOXIDE LASER, B = 5 UNITS
TRANSIENT
(g)
PICOSECONDS

Fig. 1 (cont.).

$$\int_{\Omega} \boldsymbol{T} \cdot \mathrm{d}\boldsymbol{\Omega} = -\Delta H_1 = \boldsymbol{m}^{(\mathrm{ind})} \cdot \boldsymbol{B}^{(\mathrm{em})} \qquad (11)$$

shows that the time average of ΔH_1 vanishes. Consequently, there is no simple thermodynamic averaging mechanism akin to the Langevin or Langevin–Kielich functions [48] that can be used to describe the final levels reached by the rise transients of fig. 1. In consequence these appear to be novel orientational averages which exist despite the fact that the energy ΔH_1 time averages to zero, and are therefore manifestations of an effect which cannot be described by a Langevin function.

This appears to be a generally valid result for time dependent torques of the type (2), in which a time independent induced molecular property such as $\boldsymbol{m}^{(\mathrm{ind})}$ is the arm of the torque, and the force is a component of a laser field such as $B^{(\mathrm{em})}$ whose macroscopic time average is zero. It is significant that all odd order ensemble averages such as $\langle e_{1Z} \rangle$; $\langle e_{2Z} \rangle$; and $\langle e_{3Z} \rangle$ vanish for the same FMD trajectories.

The overall conclusion drawn from data such as those in fig. 1 is that there exist orientational averages which cannot be described by the conventional Langevin functions of statistical mechanics. In the particular case of the IFE, considered here, they exist at second and higher even order only, and vanish at first and higher odd order from the same FMD trajectories. These femtosecond transients have been simulated using laser frequencies matched in the simulation with those of available, visible and infrared frequency pump lasers (table 1), and could be observed experimentally in principle with modifications of transient Kerr effect apparatus [49], primarily measurements of the extra effect of circularly polarising the pump laser on the observable femtosecond birefringence or power absorption coefficient [50].

When the ratio of tensor components in eq.

Table 2
Magnetisation m_x^2 vs. laser frequency.

Normalised magnetisation	Laser frequency (Thz)
S Bicyclopropene	
0.002 ± 0.02	30.0
0.025 ± 0.03	300.0
0.10 ± 0.03	450.0
0.55 ± 0.02	510.0
0.67 ± 0.03	540.0
0.54 ± 0.03	600.0
0.79 ± 0.03	630.0
0.76 ± 0.03	660.0
0.80 ± 0.02	750.0
0.87 ± 0.05	840.0
0.80 ± 0.05	900.0
0.88 ± 0.05	1020.0
0.80 ± 0.02	1200.0
0.65 ± 0.02	1350.0
0.28 ± 0.02	1500.0
0.00 ± 0.05	1800.0
0.50 ± 0.02	2400.0
0.90 ± 0.04	3000.0
Water	
0.05 ± 0.05	300.0
0.02 ± 0.07	500.0
0.02 ± 0.06	600.0
0.05 ± 0.03	1000.0

Table 1
Pump laser frequencies of the FMD simulations.

Pump laser	Characteristics	Frequency (THz)
Q switched CO_2	9.26–10.6 μm	~ 30
Nd^{3+}/phosphate mode locked	1056 nm, 250 MW, 2–6 ps pulse	~ 300
Rhodamine 6G dye laser, mode locked	602 nm, 50 MW, 2 ps	~ 500
Passively mode locked dye laser	503 nm, 0.5 GW, <1 ps minimum pulse	~ 600
2nd harmonic dye laser, pumped by Nd:YAG	313 nm, 1.0 MW, 15 ps	~1000

(10) is changed from 1:2:3, the time dependences of the rise transients and of the equilibrium correlation functions are changed, the details of these changes being available in the data bank. The characteristic rise time of the even order rise transients change together with the mean magnetisation at each laser frequency in table 2. These are potentially observable (see discussion) and the simulation can be used to interpret experimental observations, giving estimates of the individual component ratio of eq. (10). Note that the number of none-vanishing components depends on the molecular point group. In carbon tetrachloride, for example, there is only the scalar element of the mediating tensor, which can be determined unambiguously. Ab initio computations of the elements would be very useful, both for comparision with the experimental data and for direct use in the computer simulation, i.e. to replace arbitrary ratios.

5. Time correlation functions in the laser-on stationary state

In analysing statistically the post transient, laser-on, stationary state we are primarily seeking evidence for magnetization [1–3] in terms of fundamental molecular dynamics. This was found through the development in both types of FMD ensemble of a non-vanishing $t\rightarrow\infty$ tail in the Z component of the molecular angular momentum ACF

$$m_\infty^2 = \frac{\langle J_Z(t)J_Z(0)\rangle_{t\rightarrow\infty}}{\langle J_Z^2(0)\rangle} = \frac{\langle m_Z(t)m_Z(0)\rangle_{t\rightarrow\infty}}{\langle m_Z^2(0)\rangle} . \tag{12}$$

Here, $m_Z = \gamma J_Z$ is a magnetic dipole moment proportional to J_Z through the scalar proportionality constant γ. Values of m_∞^2 – the "dynamic magnetisation" for several different visible frequencies of the circularly polarised pump laser – are given in table 2. The normalised magnetisation in this table is defined as

$$m_\infty^2 = \frac{\langle J_Z(t)\rangle_{t\rightarrow\infty}^2}{\langle J_Z^2(0)\rangle} . \tag{13}$$

Here $\langle J_Z^2\rangle$ is the square of the $t\rightarrow\infty$ level reached by the angular momentum autocorrelation function under the influence of the torque (2) of the inverse Faraday effect, and the denominator is a normalising coefficient, the square root of the mean of the square of the angular momentum autocorrelation function, i.e. the root mean square. Note that this denominator exists at field free equilibrium, and is the standard normalising factor of the time autocorrelation function. The numerator vanishes in the absence of the laser, because in this case the mean of the angular momentum is zero in all three axes S, Y, and Z because the sample is an isotropic liquid in the laser-free condition. This quantity is a normalised magnetisation because

$$m_Z = \zeta J_Z , \tag{14}$$

and the scalar proportionality constant ζ cancels top and bottom in eq. (13). Equation (14) follows because magnetisation is proportional to the magnetic dipole moment which in turn is proportional to angular momentum, these quantities being axial vectors, positive to parity inversion and negative to motion reversal.

The normalised magnetisation of table 2 represents one of the main results of the simulation, in that it represents by computer simulation the phenomenon of magnetisation by a circularly polarised laser. Table 2 shows clearly that the magnetisation is strikingly dependent on the laser frequency for constant laser intensity, and appears both in bicyclopropene and in liquid water.

A data bank was accumulated of the complete time dependence of the angular momentum ACF responsible for m_∞^2. In general, this is

$$C_{1ij}(t) = \frac{\langle J_i(t)J_j(0)\rangle}{\langle J_i^2\rangle^{1/2}\langle J_j^2\rangle^{1/2}} , \tag{15}$$

with $i = j = X, Y, Z$ for autocorrelations and $i = j$ for cross-correlations in the laboratory frame (X, Y, Z). Components of C_1 were computed for both ensembles at up to twenty different laser frequencies. This set of functions is exemplified in the sequence of fig. 2 for liquid water for constant $E_0^2 B_0$ energetically equivalent to 2.0 kJ/mol from integration of the torque (2) over configuration in the FMD program. Figure 2 shows that the torque (2) produces an intricate variety of oscillation patterns and induces the existence of CCFs ($i = X$, $j = Y$; and $i = Y$, $j = X$) about the laser propagation direction Z.

Other extensive data sets were constructed for the orientational time correlation functions (sequence of fig. 3)

$$C_{2ij}(t) = \frac{\langle e_{1i}(t) e_{1j}(0) \rangle}{\langle e_{1i}^2 \rangle^{1/2} \langle e_{1j}^2 \rangle^{1/2}} , \tag{16}$$

and the rotational velocity correlation functions (sequence of fig. 4)

$$C_{3ij}(t) = \frac{\langle \dot{e}_{1i}(t) \dot{e}_{1j}(0) \rangle}{\langle \dot{e}_{1i}^2 \rangle^{1/2} \langle \dot{e}_{1j}^2 \rangle^{1/2}} . \tag{17}$$

The Fourier transforms of the ACFs of C_3, if observable, would be far infrared [42] power absorption coefficients, providing direct information on the dynamics of the IFE as a function of pump laser frequency and intensity.

6. Discussion

The two main results of this simulation are that the inverse Faraday effect is accompanied by hitherto unidentified orientational rise transients at second order and higher even order, and that the magnetisation predicted and observed experimentally [1–3] has been successfully simulated on a molecular basis. The transients and magnetisation can be investigated experimentally using techniques such as follow.

6.1. *Experimental configuration for the investigation of IFE transients*

The second order orientational rise transients of fig. 1 show clearly that the sample is no longer isotropic in the presence of the circularly polarised laser. If the sample were isotropic we would have

$$\langle e_{1X}^2 \rangle = \langle e_{1Y}^2 \rangle = \langle e_{1Z}^2 \rangle = \tfrac{1}{3} ,$$
$$\langle e_{1X}^4 \rangle = \langle e_{1Y}^4 \rangle = \langle e_{1Z}^4 \rangle = \tfrac{1}{5} ,$$
$$\langle e_{1X}^2 \rangle = \langle e_{2X}^2 \rangle = \langle e_{3X}^2 \rangle ,$$

and so on. This implies immediately [23] that the refractive index in the propagation axis of the laser (Z axis) becomes different from its equilibrium, laser free, value. We have

$$n(Z \text{ axis}) - n(\text{laser off}) = f(\text{rise transients}) ,$$
$$[n(Z \text{ axis}) - n(\text{laser off})]_0 = f(\langle e_{1Z}^2 \rangle_0, \ldots) , \tag{18}$$

where $\langle e_{1Z}^2 \rangle$ and so on denote the *final level* reached by the rise transient. These final levels vary from frequency to frequency, as fig. 1 demonstrates, and are accompanied on the femtosecond scale by rapid oscillations, which may fall within the time resolution of contemporary femtosecond apparatus such as that used in the optical Kerr effect [49], and which therefore may be observable directly. The physical meaning of these oscillations, which have not been predicted theoretically and which have not yet been observed experimentally, is that the laser attempts to rotate the molecular structure at the applied frequency, and the molecular ensemble attempts to respond in a way which is clearly seen visually by animation. (In this context the reader is invited to view a parallel animation by Pelkie and Evans [36] on optical NMR which illustrates this point directly. This animation was judged best of its class (natural sciences and mathematics) in the 1990 IBM Supercomputer competition, and it is available from one of the authors (Evans), the Cornell Theory Center, and IBM.) It is significant in this context that there are no first or odd order orientational transients, as expected from the structure of the torque (2), and the tensor structure of beta. This checks the FMD method for internal consistency.

The experimental configuration for the obser-

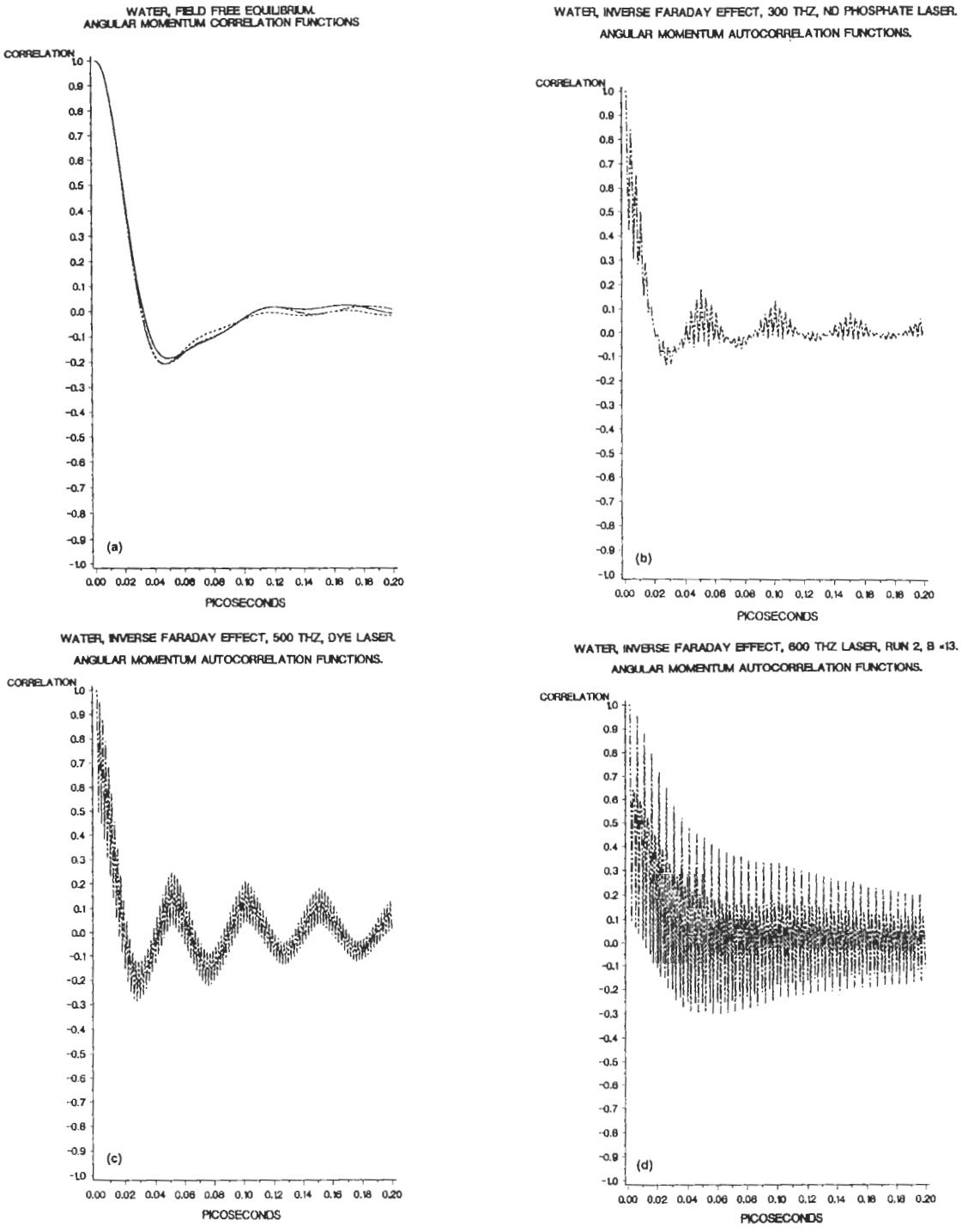

Fig. 2. Angular momentum correlation functions for water and bicyclopropene, ——— $i = j = X$; − − − $i = j = Y$; − · · − $i = j = Z$. (a) Laser free equilibrium, water; (b) Z component, 300 THz; (c) Z component, 500 THz; (d) Z component, 600 THz; (e) Z component, 1000 THz; (f) X component, 300 THz; (g) X component, 500 THz; (h) X component, 600 THz; (i) X component, 1000 THz; (j) bicyclopropene, laser free equilibrium; (k) X component, 1020 THz; (l) Z component, 1020 THz; (m) X component, 1110 THz; (n) Z component, 1110 THz; (o) Z component, 1200 THz; (p) XY component, 600 THz, cross-correlation function.

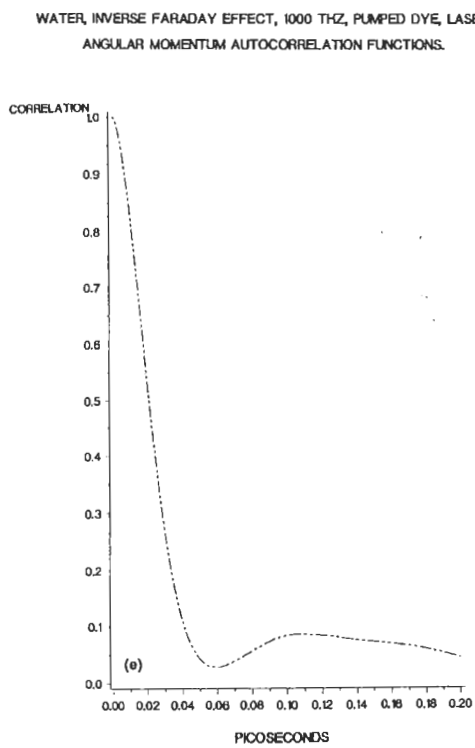
WATER, INVERSE FARADAY EFFECT, 1000 THZ, PUMPED DYE, LASER.
ANGULAR MOMENTUM AUTOCORRELATION FUNCTIONS.
CORRELATION
(e)
PICOSECONDS

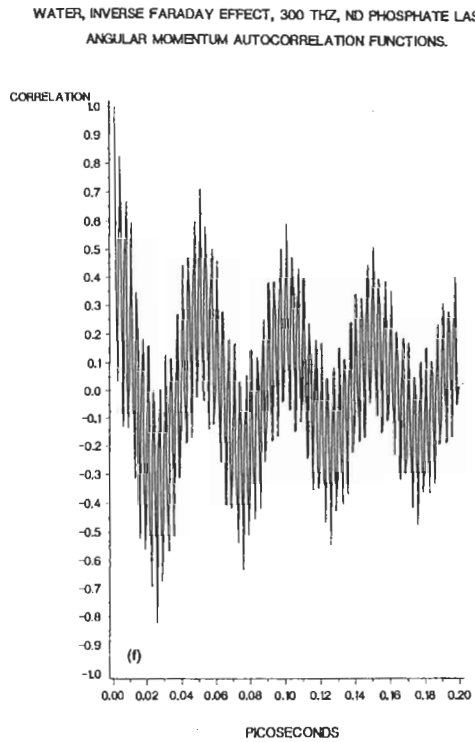
WATER, INVERSE FARADAY EFFECT, 300 THZ, ND PHOSPHATE LASER.
ANGULAR MOMENTUM AUTOCORRELATION FUNCTIONS.
CORRELATION
(f)
PICOSECONDS

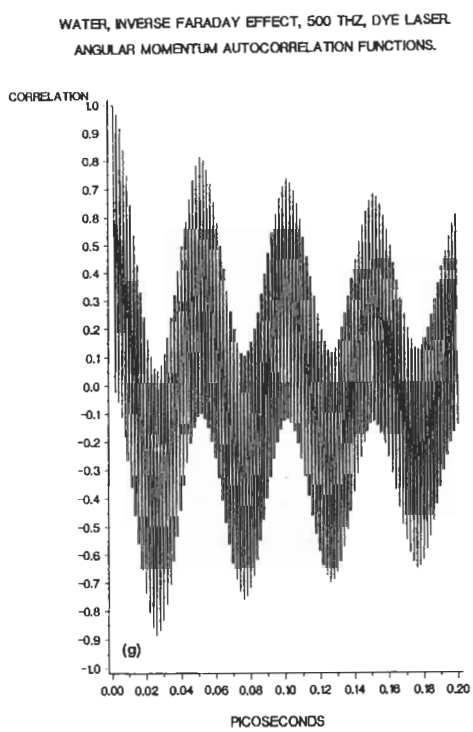
WATER, INVERSE FARADAY EFFECT, 500 THZ, DYE LASER.
ANGULAR MOMENTUM AUTOCORRELATION FUNCTIONS.
CORRELATION
(g)
PICOSECONDS

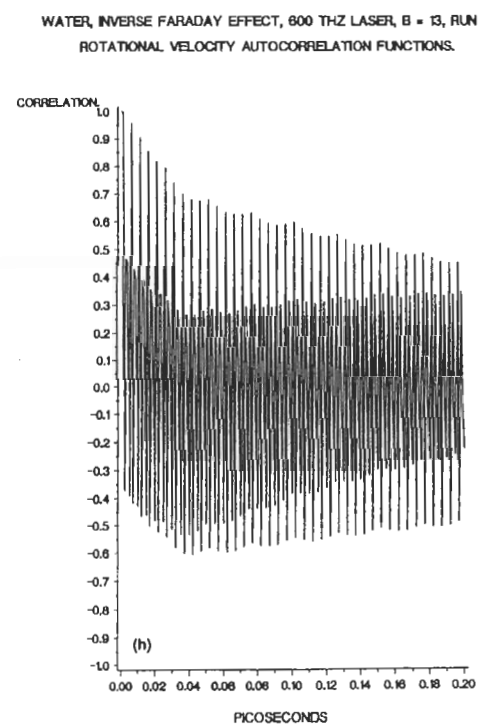
WATER, INVERSE FARADAY EFFECT, 600 THZ LASER, B = 13, RUN 2.
ROTATIONAL VELOCITY AUTOCORRELATION FUNCTIONS.
CORRELATION
(h)
PICOSECONDS

Fig. 2 (cont.).

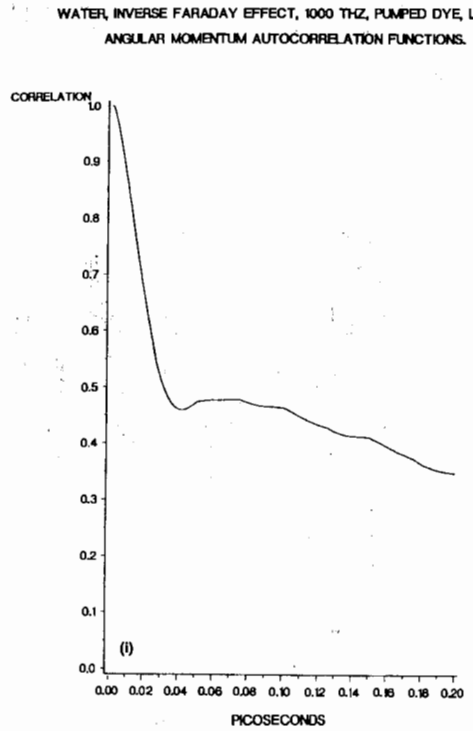
WATER, INVERSE FARADAY EFFECT, 1000 THZ, PUMPED DYE, LASER.
ANGULAR MOMENTUM AUTOCORRELATION FUNCTIONS.
CORRELATION
(i)
PICOSECONDS

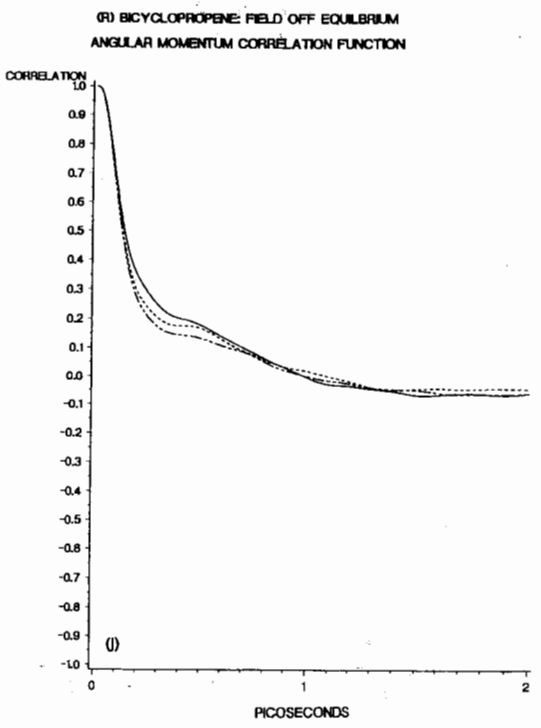
(R) BICYCLOPROPENE: FIELD OFF EQUILBRIUM
ANGULAR MOMENTUM CORRELATION FUNCTION
CORRELATION
(j)
PICOSECONDS

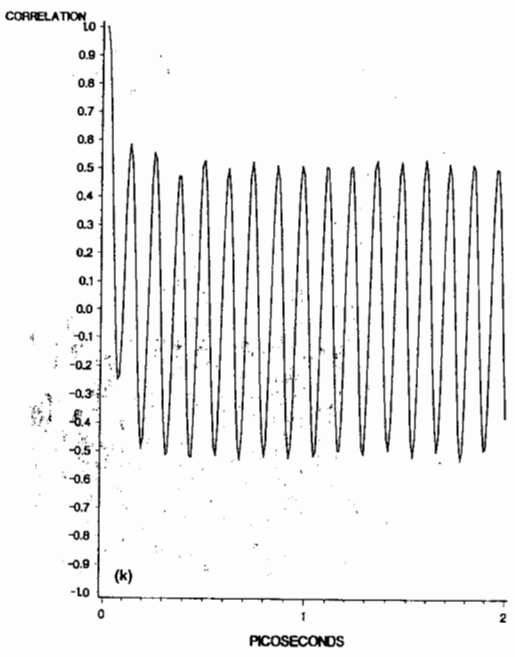
(R) BICYCLOPROPENE, THZ LASER, INVERSE FARADAY EFFECT.
ANGULAR MOMENTUM AUTOCORRELATION FUNCTIONS.
CORRELATION
(k)
PICOSECONDS

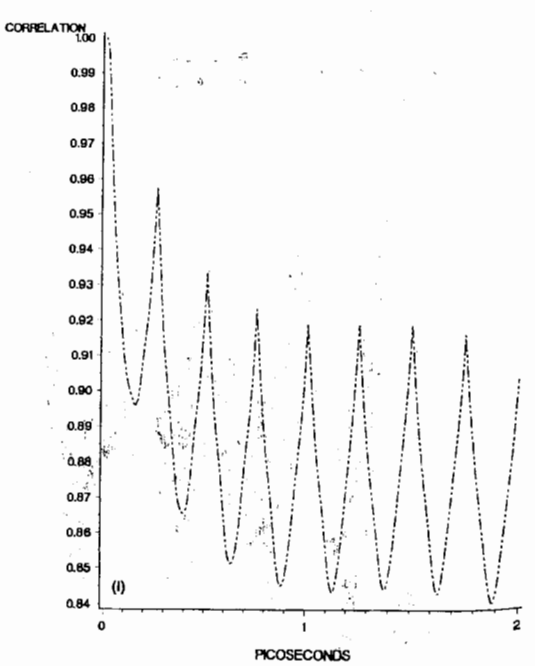
(R) BICYCLOPROPENE, THZ LASER, INVERSE FARADAY EFFECT.
ANGULAR MOMENTUM AUTOCORRELATION FUNCTIONS.
CORRELATION
(l)
PICOSECONDS

Fig. 2 (cont.).

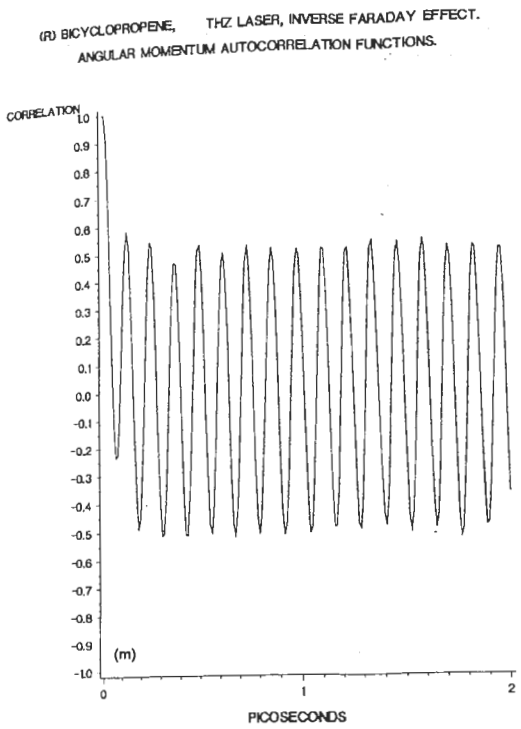
(R) BICYCLOPROPENE, THZ LASER, INVERSE FARADAY EFFECT.
ANGULAR MOMENTUM AUTOCORRELATION FUNCTIONS.
CORRELATION
(m)
PICOSECONDS

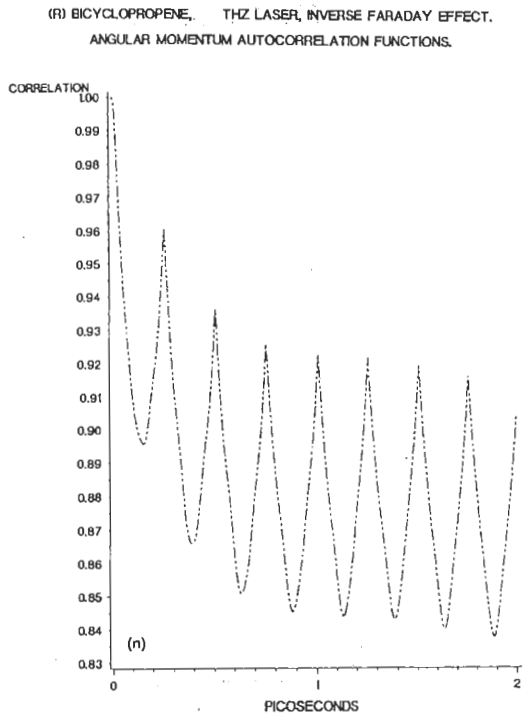
(R) BICYCLOPROPENE, THZ LASER, INVERSE FARADAY EFFECT.
ANGULAR MOMENTUM AUTOCORRELATION FUNCTIONS.
CORRELATION
(n)
PICOSECONDS

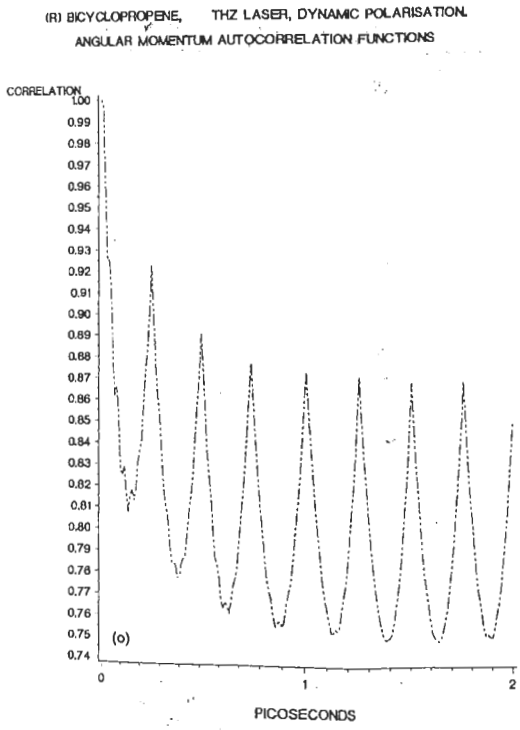
(R) BICYCLOPROPENE, THZ LASER, DYNAMIC POLARISATION.
ANGULAR MOMENTUM AUTOCORRELATION FUNCTIONS
CORRELATION
(o)
PICOSECONDS

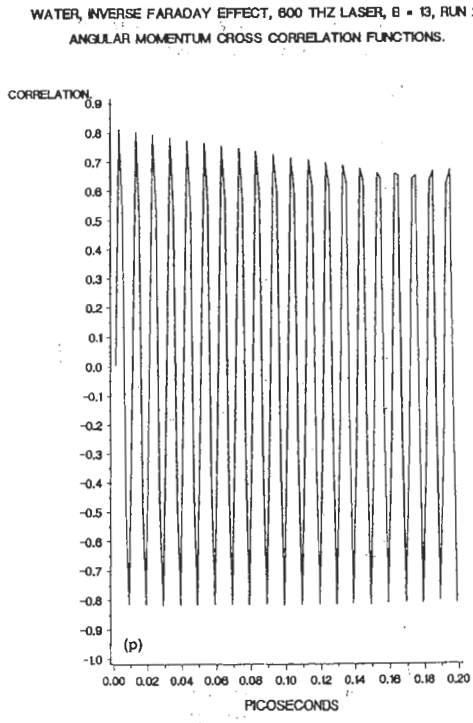
WATER, INVERSE FARADAY EFFECT, 800 THZ LASER, E = 13, RUN 2.
ANGULAR MOMENTUM CROSS CORRELATION FUNCTIONS.
CORRELATION
(p)
PICOSECONDS

Fig. 2 (cont.).

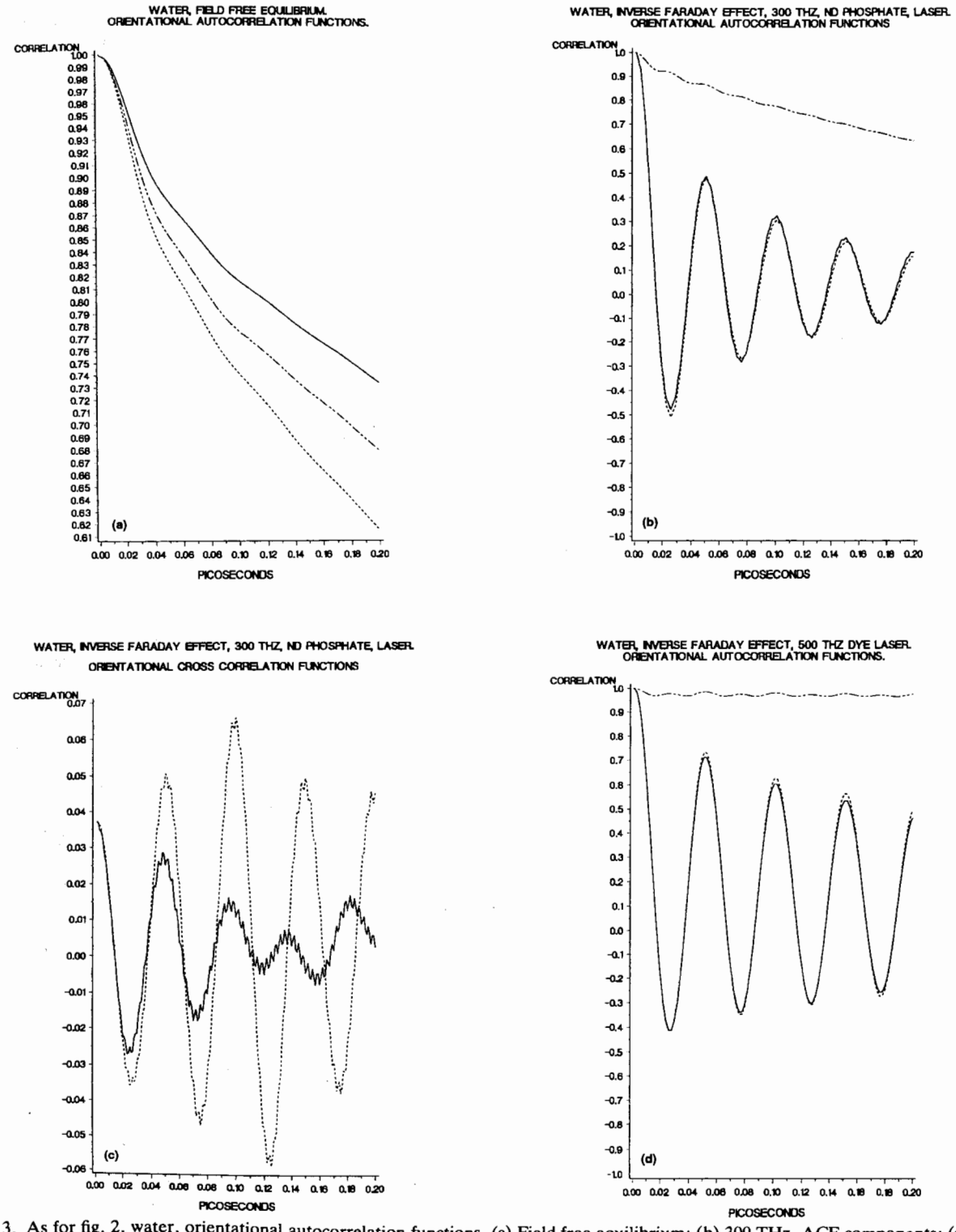

Fig. 3. As for fig. 2, water, orientational autocorrelation functions. (a) Field free equilibrium; (b) 300 THz, ACF components; (c) 300 THz, CCF components, ——— XY, – – – YX; (d) as for (b), 500 THz; (e) as for (c) 500 THz; (f) as for (b) 600 THz; (g) as for (c) 600 THz; (h) as for (b) 1000 THz; (i) as for (c) 1000 THz.

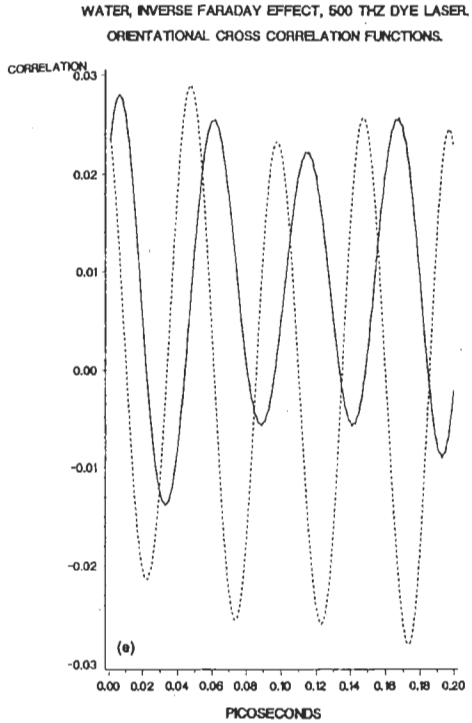
WATER, INVERSE FARADAY EFFECT, 500 THZ DYE LASER.
ORIENTATIONAL CROSS CORRELATION FUNCTIONS.
CORRELATION
0.03
0.02
0.01
0.00
-0.01
-0.02
-0.03
(a)
0.00 0.02 0.04 0.06 0.08 0.10 0.12 0.14 0.16 0.18 0.20
PICOSECONDS

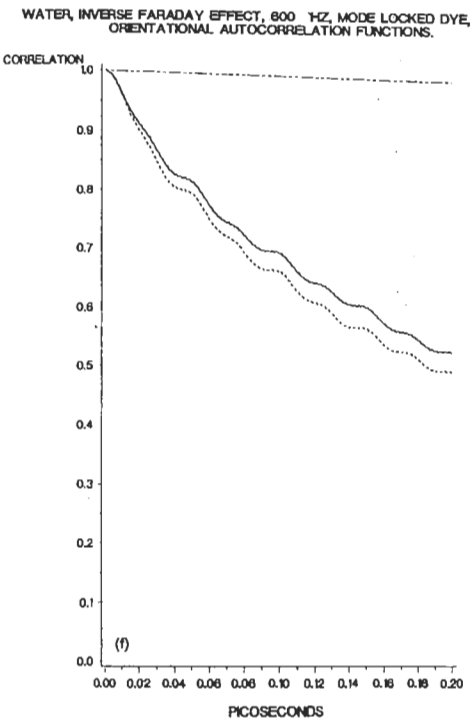
WATER, INVERSE FARADAY EFFECT, 600 THZ, MODE LOCKED DYE, LASER.
ORIENTATIONAL AUTOCORRELATION FUNCTIONS.
CORRELATION
1.0
0.9
0.8
0.7
0.6
0.5
0.4
0.3
0.2
0.1
0.0
(f)
0.00 0.02 0.04 0.06 0.08 0.10 0.12 0.14 0.16 0.18 0.20
PICOSECONDS

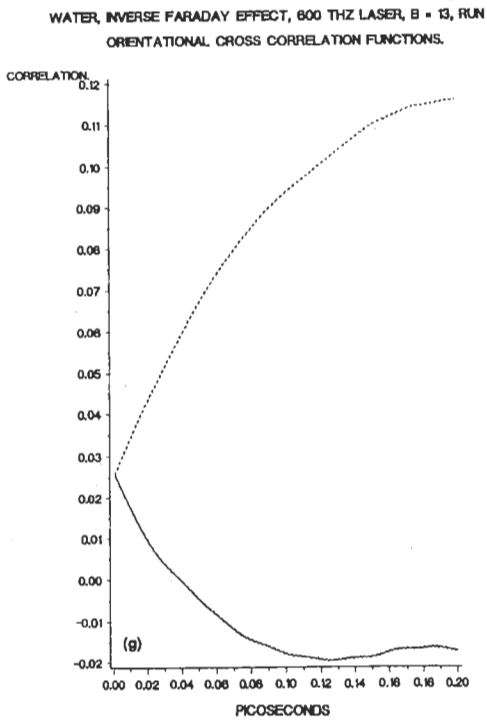
WATER, INVERSE FARADAY EFFECT, 600 THZ LASER, B = 13, RUN 2.
ORIENTATIONAL CROSS CORRELATION FUNCTIONS.
CORRELATION
0.12
0.11
0.10
0.09
0.08
0.07
0.06
0.05
0.04
0.03
0.02
0.01
0.00
-0.01
-0.02
(g)
0.00 0.02 0.04 0.06 0.08 0.10 0.12 0.14 0.16 0.18 0.20
PICOSECONDS

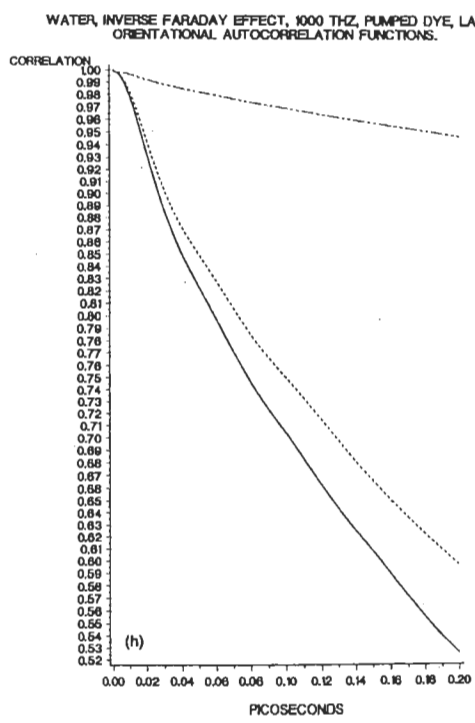
WATER, INVERSE FARADAY EFFECT, 1000 THZ, PUMPED DYE, LASER.
ORIENTATIONAL AUTOCORRELATION FUNCTIONS.
CORRELATION
1.00
0.99
0.98
0.97
0.96
0.95
0.94
0.93
0.92
0.91
0.90
0.89
0.88
0.87
0.86
0.85
0.84
0.83
0.82
0.81
0.80
0.79
0.78
0.77
0.76
0.75
0.74
0.73
0.72
0.71
0.70
0.69
0.68
0.67
0.66
0.65
0.64
0.63
0.62
0.61
0.60
0.59
0.58
0.57
0.56
0.55
0.54
0.53
0.52
(h)
0.00 0.02 0.04 0.06 0.08 0.10 0.12 0.14 0.16 0.18 0.20
PICOSECONDS

Fig. 3 (cont.).

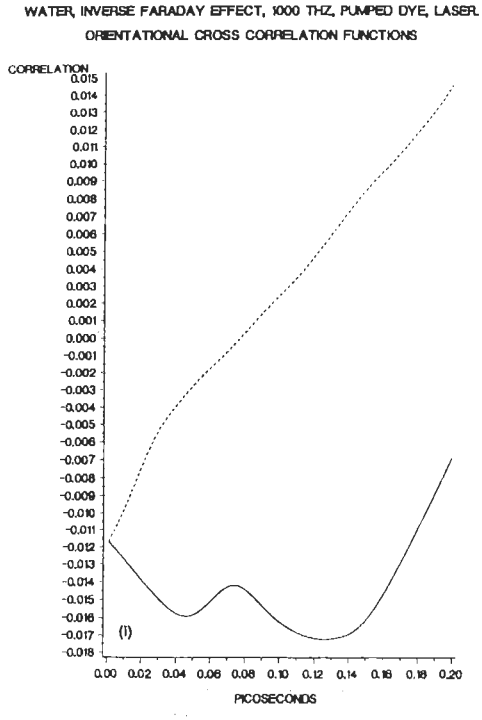

Fig. 3 (cont.).

vation of these transients therefore consists of an adaptation of contemporary femtosecond apparatus, such as that used for the optical Kerr effect [49]. The latter relies on the rotation of the plane of polarisation of a probe laser induced by a pump laser which need not be circularly polarised. The transients of fig. 1, however, show that the refractive index in the propagation axis of the pump laser becomes different from its laser-off value. In order to observe this, the pump laser must be *circularly polarised*, but the probe laser need not be polarised. The change of refractive index can be measured as a corresponding change in the power absorption coefficient, measured by the time delayed probe, on the femtosecond time scale, as in the optical Kerr effect [49]. This monitors the rise transient directly on the femtosecond time scale. The effect should vanish if the pump laser is not circularly polarised, and the change in refractive index should depend on the square of the scalar electric field amplitude of the pump laser, i.e. directly to its intensity, through a suitable Langevin function. Furthermore, the characteristic time of the rise transient shortens as the pump laser intensity is increased, a process which is described in more detail in our data bank. (The samples in fig. 1 are for the same laser intensity but different pump laser frequency.) The pump and probe lasers are parallel in this configuration, but the latter can also be directed at an angle to the pump.

As shown in ref. [39], the mediating tensor of the inverse Faraday effect is amplified when the pump laser is tuned to an optical resonance of the tensor, which is in the vicinity of the optical resonances observed in conventional magnetic circular dichroism. Under these conditions amplification should also be observable in the refractive index difference of eq. (18). Therefore a tunable circularly polarised pump laser should be used in the femtosecond apparatus, or a set of different tunable lasers covering the visible and infrared range. Samples should therefore be chosen with regard to their known MCD spectra, and in general, terms should possess large Verdet constant [2, 3]. For paramagnetics a large effect is expected with a temperature dependent component, as in the forward Faraday effect [4].

Finally, if the probe laser is linearly polarised, the inverse Faraday effect produces a rotation of its plane of polarisation, which should be observable in *addition* to the linear refractive index difference of eq. (18).

6.2. *Experimental measurement of magnetisation in the inverse Faraday effect*

Magnetisation in the inverse Faraday effect has been measured only once [2, 3] with a pulse of giant ruby laser radiation, and at only one frequency. The clear physical significance of our results in figs. 2 to 4 and in table 2 is that the magnetisation is dependent on the pump laser frequency for a given sample and laser intensity. This is a novel finding in view of the experimental data available [2, 3]. The significant technological advances made since the demonstration experiment [2, 3] point towards the need for measurement of the development of magnetisation at different laser frequencies, using

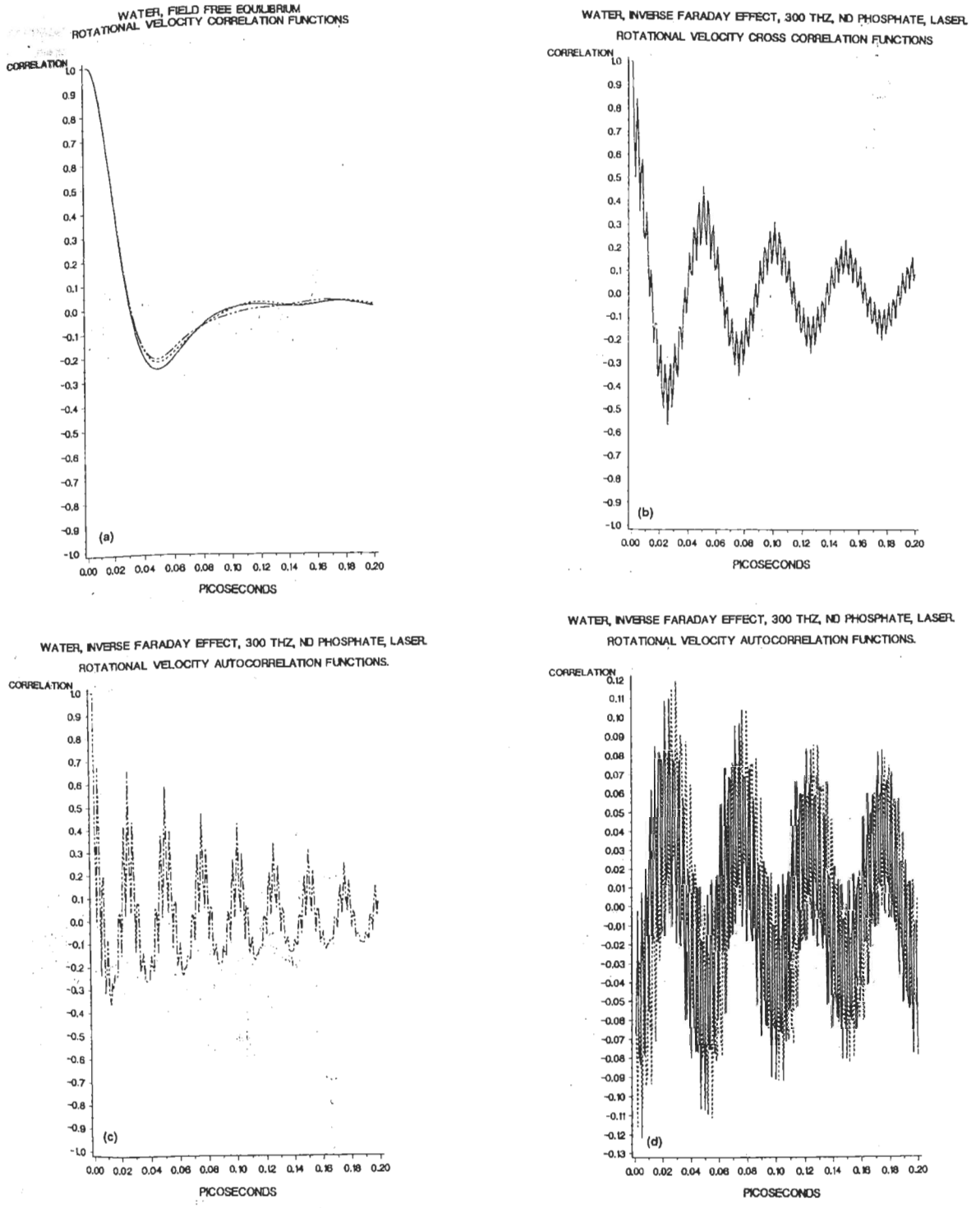

Fig. 4. As for fig. (3), rotational velocity correlation functions. (a) Field free equilibrium; (b) 300 THz, X components of ACF; (c) 300 THz, Z component of ACF; (d) CCF components as for fig. 3(c); (e) X component, 500 THz; (f) Z component, 500 THz; (g) as for (c) 500 THz; (h) X component 600 THz; (i) Z component 600 THz; (j) XY component of CCF, 600 THz; (k) YX component at 600 THz.

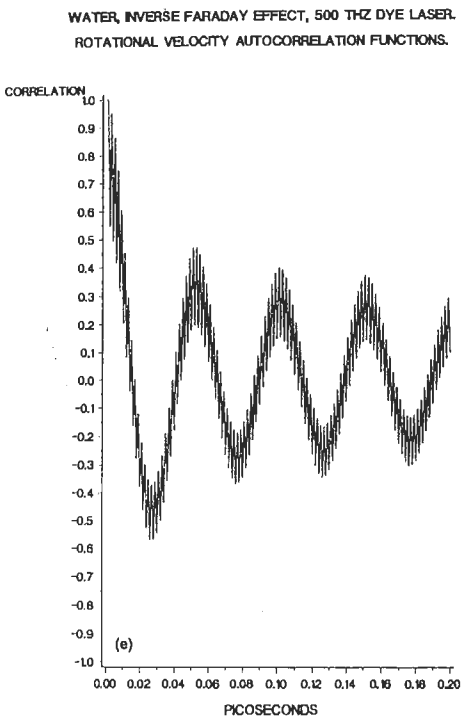
WATER, INVERSE FARADAY EFFECT, 500 THZ DYE LASER.
ROTATIONAL VELOCITY AUTOCORRELATION FUNCTIONS.
CORRELATION
(e)
PICOSECONDS

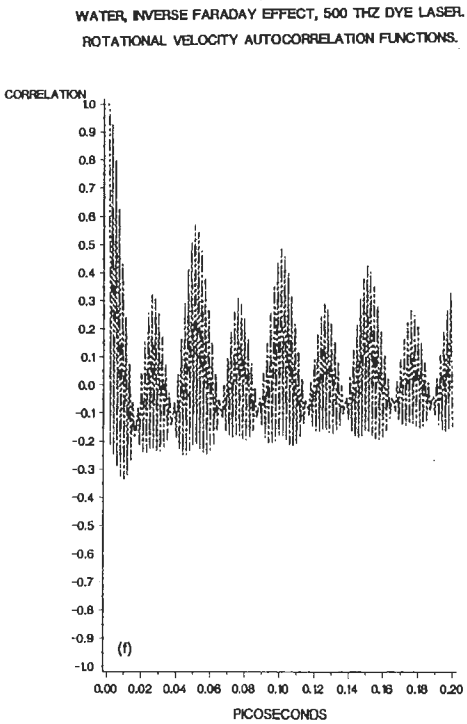
WATER, INVERSE FARADAY EFFECT, 500 THZ DYE LASER.
ROTATIONAL VELOCITY AUTOCORRELATION FUNCTIONS.
CORRELATION
(f)
PICOSECONDS

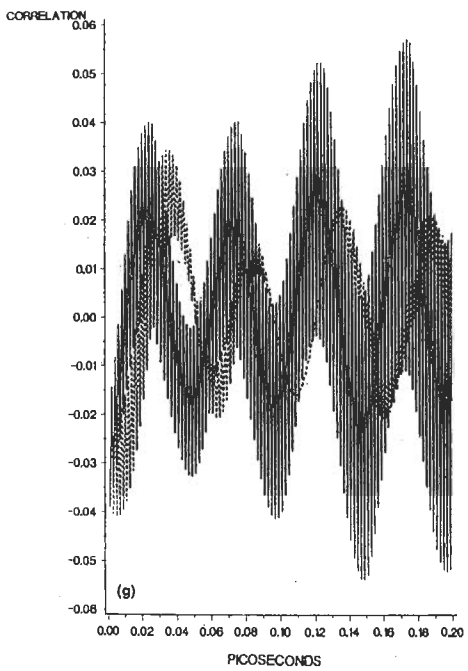
WATER, INVERSE FARADAY EFFECT, 500 THZ DYE LASER.
ROTATIONAL VELOCITY CROSS CORRELATION FUNCTIONS.
CORRELATION
(g)
PICOSECONDS

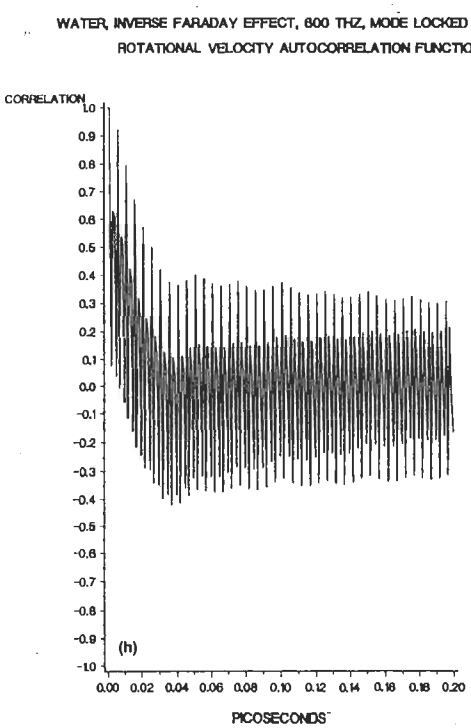
WATER, INVERSE FARADAY EFFECT, 600 THZ, MODE LOCKED DYE, LASER.
ROTATIONAL VELOCITY AUTOCORRELATION FUNCTIONS.
CORRELATION
(h)
PICOSECONDS

Fig. 4 (cont.).

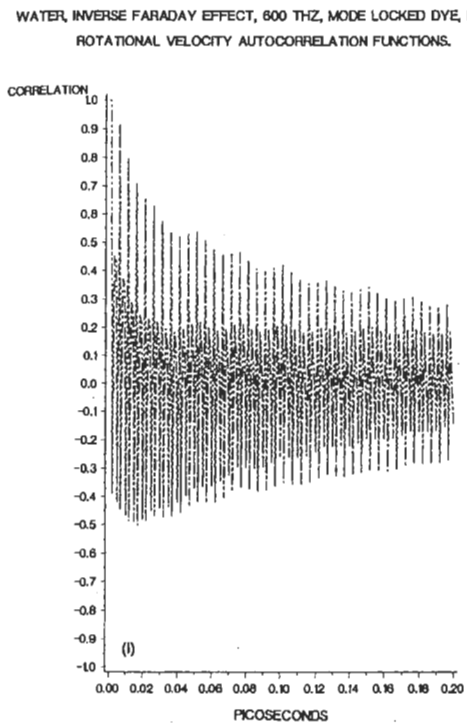
WATER, INVERSE FARADAY EFFECT, 600 THZ, MODE LOCKED DYE, LASER.
ROTATIONAL VELOCITY AUTOCORRELATION FUNCTIONS.
CORRELATION
(I)
PICOSECONDS

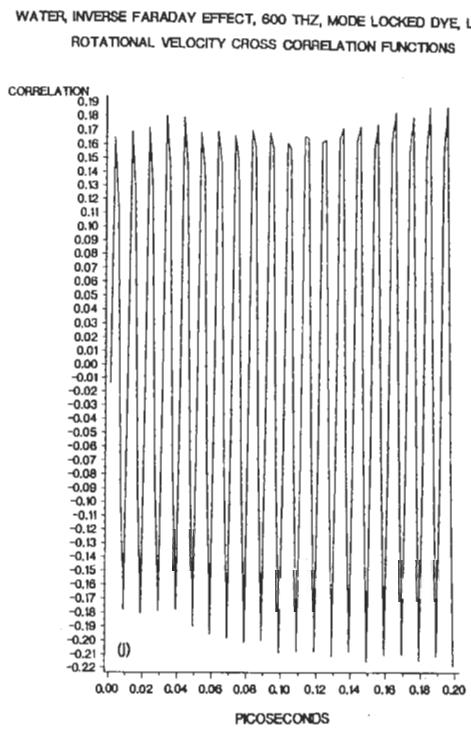
WATER, INVERSE FARADAY EFFECT, 600 THZ, MODE LOCKED DYE, LASER.
ROTATIONAL VELOCITY CROSS CORRELATION FUNCTIONS
CORRELATION
(J)
PICOSECONDS

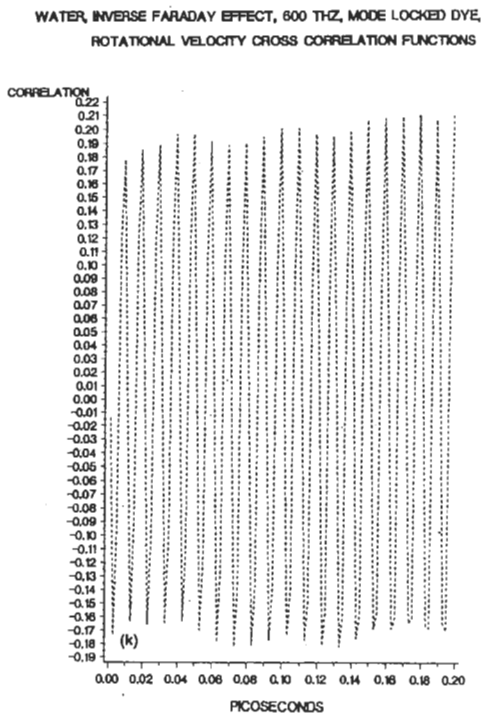
WATER, INVERSE FARADAY EFFECT, 600 THZ, MODE LOCKED DYE, LASER.
ROTATIONAL VELOCITY CROSS CORRELATION FUNCTIONS
CORRELATION
(K)
PICOSECONDS

Fig. 4 (cont.).

improvements over the original experimental method [2, 3], and also the experimental measurement of transient magnetisation on the femtosecond scale.

6.3. *Oscillation patterns of the laser-on correlation functions*

The oscillation patterns of the time correlation functions in figs. 2 to 4 are signatures of the way in which the molecular dynamics respond to the applied field, and are of fundamental interest to the Kramers theory of diffusion [24] in which the diffusion equation governing the molecular dynamics is supplemented by an external torque. The challenge to diffusion theory of the intricate oscillation patterns in figs. 2 to 4 is immediate, because the same type of torque, eq. (2), can be included in the relevant Kramers equation for solution using differential differencing [23] or reduced model theory [24]. Small changes in the laser frequency produce striking pattern changes, for example in the angular momentum correlation functions of fig. 2, and in the orientational and rotational velocity correlation functions of figs. 3 and 4. These patterns should emerge consistently from diffusion theory.

The Fourier transforms of the various patterns in figs. 3 and 4 are related [42] to dielectric loss and far infrared and infrared to visible frequency power absorption coefficients, respectively. Contemporary Fourier transform spectrometers can take a spectrum across the entire range from far infrared to visible in a matter of microseconds, and it appears possible to design a pump pulse which is longer than this, thus allowing a spectrum to be taken as the pulse passes through the sample. This process can be repeated several thousand times and averaged, to produce a relatively noise-free Fourier transform of the patterns in fig. 4. This Fourier transform can also be obtained by simulation, forging another point of comparison between experiment and theory.

There appears to be a considerable amount of new physics in figs. 2 to 4, therefore, in the form of patterns of correlation between dynamical variables formed by the passage of an intense, circularly polarised laser pulse which sets up the torque (2). These patterns are intricately dependent on laser frequency, and this provides a wealth of data with which to test the efficacy of the model of the intermolecular potential used in the simulation. It may become possible in future work to repeat the hundreds of runs completed in the course of this work with different model potentials, such as the MCYL for water [46]. The present water potential has been compared already [46] with the MCYL, and in general, the extra vibrational content of MCYL does not affect significantly the majority of the autocorrelation functions, but MCYL does modify those cross-correlation functions which are directly dependent on vibration. A full comparison of this aspect is in the literature [46]. It is desirable also to repeat the present analysis with different molecular symmetries and scalar elements of the mediating tensor. A limited analysis in this context during the course of this work has shown that the transients, correlation functions, and their oscillation patterns are all functions of the scalar elements of the mediating tensor of the inverse Faraday effect.

Acknowledgements

The Swiss NSF and the Canton and University of Zurich are thanked for support for ME and SW, respectively. Animation for this paper was carried out at Cornell Theory Center, which receives major funding from the US NSF, IBM (US), the State of New York, and the Corporate Research Institute. Dr. Laura J. Evans is thanked for invaluable help with the SAS plotting facility of the Irchel mainframe. ETH Zurich is thanked for a generous grant of time on the IBM 3090 supercomputer, with which the FMD simulations were carried out.

References

[1] P.S. Pershan, Phys. Rev. 130 (1963) 919.
[2] J.P. van der Ziel, P.S. Pershan and L.D. Malmstrom, Phys. Rev. Lett. 15 (1965) 190.

[3] P.S. Pershan, J.P. van der Ziel and L.D. Malmstrom, Phys. Rev. 143 (1966) 574.
[4] L.D. Barron, Molecular Light Scattering and Optical Activity (Cambridge Univ. Press, Cambridge, 1982).
[5] P.W. Atkins and M.H. Miller, Mol. Phys. 15 (1968) 503.
[6] P.W. Atkins, Molecular Quantum Mechanics, 2nd. Ed. (Oxford Univ. Press, Oxford, 1983).
[7] Y.R. Shen, The Principles of Non-Linear Optics (Wiley Interscience, New York, 1984).
[8] S. Feneuille, Rep. Prog. Phys. 40 (1977) 1257.
[9] D.C. Hanna, M.A. Yuratich and D. Cotter, Non-Linear Optics of Free Atoms and Molecules (Springer, New York, 1979).
[10] H.R. Gray and C.R. Stroud, Jr., Opt. Commun. 25 (1978) 359.
[11] G. Wagnière, Phys. Rev. A 40 (1989) 2437.
[12] S. Woźniak, G. Wagnière and R. Zawodny, Phys. Lett. A 154 (1991) 259.
[13] S. Woźniak and R. Zawodny, Phys. Lett. A 85 (1981) 111.
[14] S. Woźniak, B. Linder and R. Zawodny, J. de Phys. 44 (1983) 403.
[15] S. Woźniak and R. Zawodny, Acta Phys. Polon. 61A (1982) 175.
[16] M.W. Evans, Phys. Rev. Lett. 64 (1990) 2909.
[17] M.W. Evans, Opt. Lett. 15 (1990) 863.
[18] M.W. Evans, Physica B 168 (1991) 9.
[19] M.W. Evans, J. Mol. Spect. 143 (1990) 327.
[20] M.W. Evans, J. Phys. Chem. 95 (1991) 2256.
[21] M.W. Evans, J. Chem. Phys. 76 (1982) 5473, 5480.
[22] M.W. Evans, J. Chem. Phys. 77 (1982) 4632; 78 (1983) 925.
[23] M.W. Evans, W.T. Coffey and P. Grigolini, Molecular Diffusion (Wiley Interscience, New York, 1984; MIR, 1988).
[24] M.W. Evans, P. Grigolini, G. Pastori, I. Prigogine and S.A. Rice, eds., Advances in Chemical Physics, Vol. 62 (Wiley Interscience, New York, 1985).
[25] W.T. Coffey, ref. [24].
[26] M.W. Evans, G.C. Lie and E. Clementi, Phys. Lett. A 130 (1988) 289.
[27] M.W. Evans, I. Prigogine and S.A. Rice, Advances in Chemical Physics, Vol. 63 (Wiley Interscience, New York, 1985).
[28] M.W. Evans, G.C. Lie and E. Clementi, Z. Phys. D 7 (1988) 397.
[29] M.W. Evans, in: Advances in Chemical Physics, Vol. 81, eds. I. Prigogine and S.A. Rice (Wiley Interscience, New York, 1991) in press.
[30] M.W. Evans, Phys. Rev. A 39 (1989) 6041.
[31] M.W. Evans and D.M. Heyes, Mol. Phys. 65 (1988) 1441.
[32] L.D. Barron, in: New Developments in Molecular Chirality, ed. P.G. Mezey (Reidel, Dordrecht, 1990).
[33] M.W. Evans, G.C. Lie and E. Clementi, J. Chem. Phys. 87 (1987) 6040.
[34] M.W. Evans, Phys. Rev. A 41 (1990) 6041.
[35] M.W. Evans and G. Wagnière, Phys. Rev. A 42 (1990) 6732.
[36] M.W. Evans, S. Woźniak and G. Wagnière, Physica B 173 (1991) 357.
[37] E. Clementi, ed., MOTECC 89 (Escom, Leiden, 1989).
[38] E. Clementi, ed., MOTECC 90 (Escom, Leiden, 1990).
[39] S. Woźniak, M.W. Evans and G. Wagnière, Mol. Phys., in press.
[40] M.W. Evans, S. Woźniak and G. Wagnière, Physica B 175 (1991) 412.
[41] S. Kielich, in: Dielectric and Related Molecular Processes, Vol. 1, M. Davies (Senior Reporter) (Chem. Soc., London, 1972).
[42] M.W. Evans, G.J. Evans, W.T. Coffey and P. Grigolini, Molecular Dynamics (Wiley Interscience, New York, 1982) Ch. 1.
[43] Software packages of refs. [37] and [38].
[44] Daresbury Program Library of the Science and Engineering Research Council's Daresbury Laboratory, near Warrington, UK, available on request for non-profit use.
[45] M.W. Evans, J. Mol. Liq. 34 (1987) 269.
[46] M.W. Evans, K.N. Swamy, K. Refson, G.C. Lie and E. Clementi, Phys. Rev. A 36 (1988) 3935.
[47] M.W. Evans, G.C. Lie and E. Clementi, J. Chem. Phys. 88 (1988) 5157.
[48] S. Kielich, Nonlinear Molecular Optics (Nauka, USSR, 1981).
[49] C. Kalpouzos, D. McMorrow, W.T. Lotshaw and G.A. Kenney-Wallace, Chem. Phys. Lett. 150 (1988) 138.
[50] J. Jortner, R.D. Levine, I. Prigogine and S.A. Rice, eds., Advances in Chemical Physics, Vol. 47, Pts. 1 and 2 (Wiley Interscience, New York, 1981).